
ELSEVIER
VOLUME 145
5 APRIL 2014
ISSN 0034-4257
Remote Sensing of Environment
http://www.elsevier.com/locate/rse

Remote Sensing of Environment 145 (2014) 93–104

Contents lists available at ScienceDirect

Remote Sensing of Environment

journal homepage: www.elsevier.com/locate/rse

Airborne multi-temporal L-band polarimetric SAR data for biomass estimation in semi-arid forests

Mihai A. Tanase [a,*], Rocco Panciera [a], Kim Lowell [a], Siyuan Tian [a], Jorg M. Hacker [b], Jeffrey P. Walker [c]

[a] Cooperative Research Centre for Spatial Information, The University of Melbourne, Australia
[b] Airborne Research Australia, School of the Environment, Flinders University, Australia
[c] Department of Civil Engineering, Monash University, Australia

ARTICLE INFO

Article history:
Received 23 April 2013
Received in revised form 23 January 2014
Accepted 27 January 2014
Available online 22 February 2014

Keywords:
Forest biomass
L-band radar
Multi-temporal
Polarimetric decomposition
Random forest
Forest variability

ABSTRACT

Using the airborne Polarimetric L-band Imaging Synthetic aperture radar (PLIS) the impact of high revisit cycle and full polarimetric acquisitions on biomass retrieval was investigated by means of backscatter-based multi-temporal methods. Parametric and non-parametric models were used to relate reference biomass levels obtained from field plot measurements and high point density lidar data to backscatter intensities or polarimetric target decomposition components. Single-date retrieval using multiple independent variables provided lower estimation errors when compared to models using one independent variable with errors decreasing by 2% to 15%. The multi-temporal aggregation of daily biomass estimates did not improve the overall retrieval accuracy but provided more reliable estimates with respect to single-date methods. Backscatter intensities improved estimation accuracies up to 10% compared to polarimetric target decomposition components. Using all four polarizations increased the estimation accuracy marginally (2%) when compared to a dual-polarized system. The biomass estimation error was considerably reduced (up to 30%) only by decreasing the spatial resolution and was related to decreasing forest variability with increasing pixel size. These results indicate that, at least in semi-arid areas, future L-band missions would not significantly improve biomass estimation accuracy using backscatter-based modeling approaches despite their better spatial resolution, higher revisit cycles and the availability of fully polarimetric information.

1. Introduction

The past decades have witnessed an unprecedented development of remote sensing techniques for land monitoring. Passive sensors had a head start with the launch of the first Landsat satellite early in the 1970's. The development of active sensors such as synthetic aperture radar (SAR) was slower with the first missions being launched in the early 1990s. The first space borne platforms carried single-band single-polarization sensors with the European Remote Sensing (ERS) satellite, Japanese Earth Resource Satellite-1 (JERS-1) and Radar satellite (RADARSAT-1) among the pioneer SAR satellites. The subsequent satellite-borne sensors had improved characteristics, such as multiple polarizations, different acquisition modes, and higher spatial resolutions. Recently, the use of SAR constellations has significantly increased the revisit cycle (e.g., Cosmo Sky-Med) or simultaneously acquired data with multiple spacecrafts (i.e., TerraSAR/TanDEM-X mission). The increasing availability of SAR data has enabled research in numerous fields which has in turn led to the development of diverse applications such as ship detection (Eldhuset, 1996), earth displacement measurements (Yague-Martinez, Eineder, Xiao Ying, & Minet, 2012), sea-ice mapping (Curlander, Holt, & Hussey, 1985), fire impact assessment (Tanase, de la Riva, Santoro, Le Toan, & Perez-Cabello, 2010; Tanase, Santoro, Wegmüller, de la Riva, & Perez-Cabello, 2010), land-use change detection (Tanase, Le Toan, de la Riva, & Santoro, 2009) and biomass estimation (Dobson, Pierce, Sarabandi, Ulaby, & Sharik, 1992; Englhart, Keuck, & Siegert, 2011; Morel et al., 2011; Rignot, Zimmermann, & van Zyl, 1995; Robinson, Saatchi, Neumann, & Gillespie, 2013; Santoro, Eriksson, Askne, & Schmullius, 2006; Tanase et al., in press).

Biomass estimation is undoubtedly one of the most pressing research topics currently, since information on forest spatial distribution, biomass levels and dynamics is needed for accurate greenhouse gases flux estimation, and thus policy development and implementation (Gibbs, Brown, Niles, & Foley, 2007). The last two decades have been strongly focused on the extraction of forest biomass estimates from SAR data, with the most recent research employing L-band data due to its greater sensitivity to biomass levels and the data availability from satellite missions such as JERS-1 and Advanced Land Observing Satellite (ALOS) Phased Array type L-band Synthetic Aperture Radar (PALSAR) (Morel et al., 2011; Santoro et al., 2006; Santoro et al., 2009). The potential of L-band radar backscatter to estimate aboveground biomass (AGB) has been studied for most forest types, ranging from boreal to tropical regions using airborne and/or space borne sensors (Harrell, Bourgeau-Chavez, Kasischke, French, & Christensen, 1995; Imhoff, 1995; Kasischke, Christensen, & Bourgeau-Chavez, 1995; Le Toan, Beaudoin, & Guyon,

* Corresponding author at: The University of Melbourne.
E-mail address: mihai@tma.ro (M.A. Tanase).

0034-4257/$ – see front matter © 2014 Elsevier Inc. All rights reserved.
http://dx.doi.org/10.1016/j.rse.2014.01.024

1992; Lucas et al., 2010; Pulliainen, Kurvonen, & Hallikainen, 1999; Santoro et al., 2006).

A number of biomass retrieval strategies were adopted including initially empirical (Harrell, Kasischke, Bourgeau-Chavez, Haney, & Christensen, 1997; Lucas, Milne, Cronin, Witte, & Denham, 2000; Ranson, Saatchi, & Sun, 1995; Sandberg, Ulander, Fransson, Holmgren, & Le Toan, 2011), subsequently semi-empirical (Lu, 2006; Pulliainen, Mikkela, Hallikainen, & Ikonen, 1996; Santoro et al., 2006) and, more recently numerical (Burgin, Clewley, Lucas, & Moghaddam, 2011; Lucas, Moghaddam, & Cronin, 2004) models. The empirical models have related radar backscatter to AGB using a range of functional forms, including linear (Sandberg et al., 2011), logarithmic (Moreau & Le Toan, 2003), exponential (Englhart et al., 2011; Moreau & Le Toan, 2003) and higher degree polynomials (Dobson, Ulaby, Le Toan, Beaudoin, & Kasischke, 1992), while semi-empirical models have frequently been based on the water cloud model (Attema & Ulaby, 1978). Machine learning algorithms adapted to regression problems were also recently used for the retrieval of bio-geophysical parameters from polarimetric SAR data (Neumann, Saatchi, Ulander, & Fransson, 2012). Although consensus on the best models for biomass retrieval is yet to emerge, parametric models are frequently used (Harrell et al., 1995; Harrell et al., 1997; Neumann et al., 2012; Robinson et al., 2013; Saatchi, Halligan, Despain, & Crabtree, 2007; Saatchi, Houghton, Dos Santos, Soares, & Yu, 2007; Saatchi, Marlier, Chazdon, Clark, & Russell, 2011; Sandberg et al., 2011).

In recent years, polarimetric interferometry, tomography and polarimetric coherence tomography have been used to estimate forest characteristics such as height or vertical structure (Cloude, 2006, 2007; Cloude & Papathanassiou, 1998). Such methods have shown promising results but their implementation at wider scale has remained limited due to the lack of suitable satellite sensors or observation scenarios (Garestier, Dubois-Fernandez, & Papathanassiou, 2008; Hajnsek, Kugler, Lee, & Papathanassiou, 2009; Tebaldini & Rocca, 2012). Their potential also remains to be demonstrated over a wide range of forest conditions and especially in semi-arid areas where trees are generally small and significant penetration through canopy gaps occurs (Cronin, 2004; Le Toan et al., 1992; Rignot et al., 1995).

L-band SAR sensors cannot measure biomass directly since the backscattered waves interact mostly with the canopy layer (leaves/needles and branches), which contains only a fraction of the total tree biomass. However, canopy biomass is often a reliable indicator of total tree biomass, allowing for indirect relationships to be formed between radar and forest inventory data. Fully polarized radar datasets have the advantage of enabling a complete description of the scattering process, thus providing information on the entire scattering matrix which can be decomposed into ground, volume, and ground–volume contributions, thus allowing some of the vertical forest structure to be retrieved. It is assumed that such information better relates to forest biomass since the influence of the underlying ground is reduced for some of these components. Coherent polarimetric decompositions can separate the scattering matrix into simpler scattering responses. However, since the scattering matrix is only able to characterize pure scatterers, such decompositions are less useful for the characterization of distributed scatterers, such as forests, due to the presence of speckle noise. Forested areas are better characterized using second order (i.e., covariance or coherency matrices) polarimetric representations through incoherent, model-based decompositions (Cloude & Pottier, 1996). The Freeman–Durden decomposition (Freeman & Durden, 1998) was among the first developed for separating three scattering components related to surface, double bounce and volume scattering using physical models. A fourth component was later added (Yamaguchi, Moriyama, Hiroyoshi, & Shinji, 2005) to compensate for limitations in the Freeman–Durden model for areas with topographic slope. Recently, both methods have been reformulated (van Zyl, Arii, & Kim, 2011) to avoid nonphysical negative powers obtained for some polarization combinations.

In the near future new sensors with greater capabilities will be deployed, both to replace aging/defunct sensors, and to create new constellations. With the next generation L-band SAR sensors featuring improved spatial resolution (down to 3 m in range and 1 m in azimuth), higher revisit cycles (down to eight days), and fully polarized acquisitions, there is a need to evaluate to what extent such capabilities could improve the biomass estimation accuracy using current or novel (i.e., multi-temporal) backscatter-based modeling approaches. Although a variety of polarimetric model-based decomposition techniques are currently available, the limited availability of fully polarized datasets has restricted their use and validation under a wide range of forest and environmental conditions. Similarly, limited availability of high temporal frequency SAR datasets has restricted the development of multi-temporal biomass retrieval techniques based on dense data series. Most polarimetric decomposition studies were undertaken for classification purposes (Dong, Milne, & Forster, 2001; Maghsoudi, Collins, & Leckie, 2012; Trisasongko, 2010) rather than direct biomass estimation (Gonçalves, Santos, & Treuhaft, 2011). To the knowledge of the authors, the use of specific scattering components for model parameterization and direct biomass estimation has only been investigated recently (Neumann et al., 2012), while biomass estimation from dense multi-temporal polarimetric SAR data series remains to be explored. Consequently, the objectives of this study were to: i) evaluate whether improved forest biomass estimates can be obtained from high temporal frequency SAR data as opposed to single date retrieval algorithms in semi-arid environments, ii) investigate the use of polarimetric target decomposition components for direct model parameterization, and iii) assess the impact of available polarizations and forest variability on the biomass retrieval error.

2. Study area and ground data

The study area is located in the western plains of the Murrumbidgee catchment, a semi-arid environment, near the township of Narrandera, New South Wales, Australia (Fig. 1). The area is characterized by agricultural and grazing farms interspersed with forests. The precipitation is evenly distributed throughout the year with a mean annual rainfall of 440 mm. The mean maximum temperature is 33 °C and occurs in January while the mean minimum temperature is 3 °C and occurs in July. A small forest area, approximately 1800 ha in size, and dominated by white cypress pine (*Callitris glucophylla*) with dispersed (10%) grey box trees (*Eucalyptus microcarpa*) was the focus of this investigation. The topography is nearly flat with elevation ranging from 140 m to 190 m and slopes being less than 5° for most of the forest.

A biometric survey was conducted using 60 circular plots (500 m^2 each, 12.62 m in radius) clustered in 12 sites, with the data collected in September 2011 (Fig. 1 and Appendix A). A cluster site consisted of a central plot with four surrounding plots whose centers were spaced at a distance of 35 m in the cardinal directions. The GPS coordinates, diameter and height were recorded for 2251 trees with a diameter at breast height (dbh) of 5 cm and above, whereas smaller trees were counted and only their average height recorded. Information on grass cover and average height was also collected for 10 additional plots that have relatively sparse vegetation. The biomass of the trunk, branches and leaves as well as the total AGB were estimated for each tree using species-specific allometric equations (Burrows, Hoffman, Compton, & Back, 2001; Hamilton, Brodie, & O'Dwyer, 2005). These values were subsequently aggregated to plot level. For white cypress pine both dbh- and height-based allometric equations were considered. The only equations available for this species (Burrows et al., 2001) were developed for the south-central Queensland region (1000 km north of the study area) which is characterized by higher annual average precipitations (600 mm). Since the Burrows' models consistently overestimated tree heights as a function of tree diameter for this study area (Fig. 2), the biomass values obtained from dbh- and height-based allometric equations were averaged. The total AGB for individual plots varied between 1.5 and 179.5 Mg ha^{-1}.

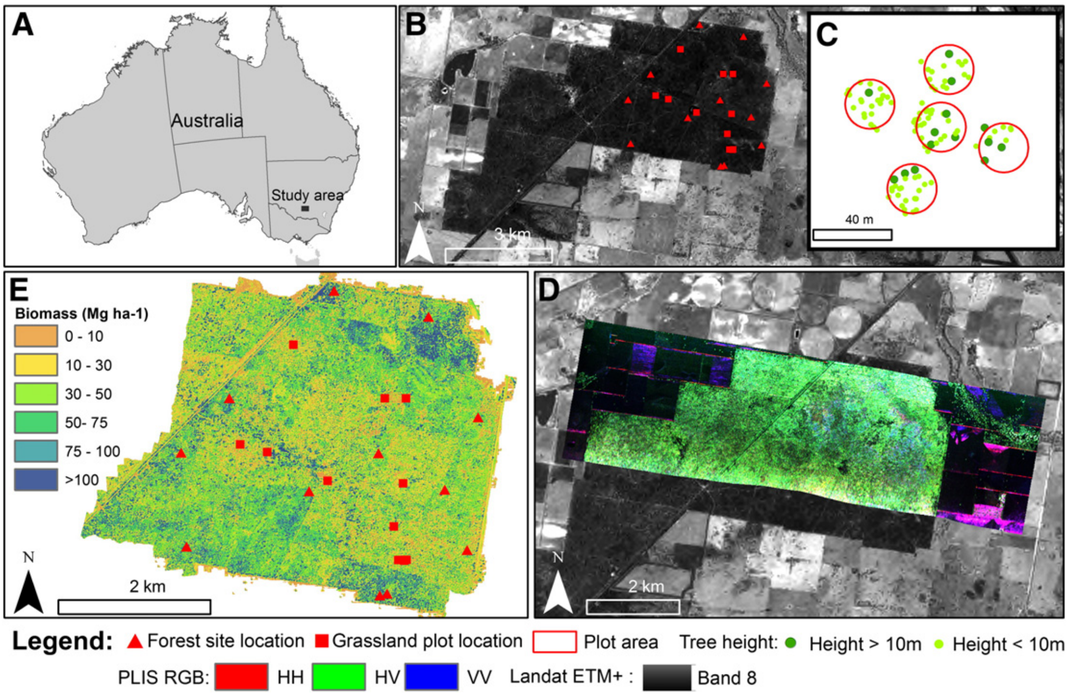

Fig. 1. Study area (black square in panel A) and field data sampling locations (B) together with the airborne data acquired by the PLIS (D) sensor. The inset (C) shows the separation of sampled plots at each site, the tree height and the position of the trees measured in the field for an example site. Panels B and D have as the background a Landsat ETM + panchromatic image acquired on 24 October 2003. Panel E presents the reference biomass map obtained from filed plots and Lidar data through multiple regression.

Ancillary information on soil moisture, soil roughness, wood density and leaf water content was also collected during the field campaign for several sites. Soil moisture decreased from the beginning to the end of the campaign by an average of 7% while leaf water content decreased by 30%. Trunk water content was relatively stable (around 35%) during the second half of the campaign when such measurements were taken. The average surface roughness was 0.7 cm with a standard deviation of 0.27 cm across eight sites where measurements were taken using a 1-m long contact profiler.

3. Remote sensing data

The remote sensing data were acquired in the context of the Soil Moisture Active Passive Experiment (SMAPEx), which was focused on providing airborne and ground data for algorithm development for the upcoming NASA Soil Moisture Active Passive mission (Panciera et al., 2013). Although the SMAPEx experiment consisted of three different field campaigns undertaken in 2010 and 2011, the forest survey and over-flights were only carried out during SMAPEx3 (5–23 September 2011). The present study only uses data from two of the sensors that acquired airborne information during these campaigns: the Polarimetric L-band Imaging Synthetic aperture radar (PLIS) and the Riegl Airborne Laser Scanning (ALS) Q560 (Hug, Ullrich, & Grimm, 2004).

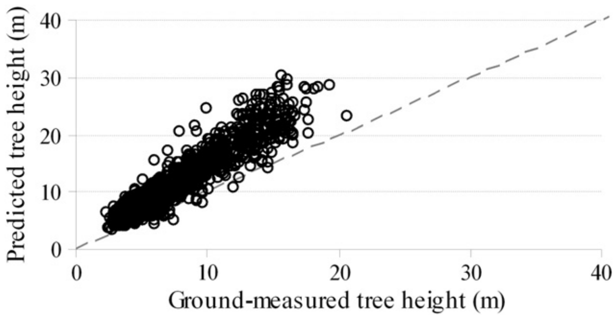

Fig. 2. Observed vs. predicted height for white cypress pine. The predicted height was computed as a function of dbh using Burrows et al. (2001) allometric equations. The dashed line is the 1:1 line that indicates perfect agreement.

3.1. SAR data

The PLIS is a full polarimetric sensor with a radar frequency of 1.26 GHz which uses micro-strip antennas mounted either underneath or on the wings of light aircrafts. Typically, PLIS operates between 300 and 3000 m aboveground level at aircraft speeds of 40–120 m/s with a pulse repetition frequency between 2 and 8 kHz. Using a dual channel receiver both H and V polarizations are sampled simultaneously. The sensor illuminates the ground on either side of the aircraft with an incidence angle varying from 15° to 45° across the swath. Using a 30 MHz bandwidth, the single look slant range resolution is 6 m. The azimuth resolution is 0.8 m. More information about the PLIS sensor is found in Gray et al. (2011). During the SMAPEx3 campaign the sensor was flown over the study area nine times with a temporal frequency of two to three days. However, in one of the flights (18 September 2012) the GPS timestamp over the forest was not correctly recorded and the data could not be processed which left only eight days available for analysis (Table 1). The sensor was flown at an altitude of 3000 m, giving a nominal ground swath of 2200 m on either side of the aircraft.

The PLIS polarimetric calibration was accomplished using a modified version (Goh, Preiss, Gray, & Stacy, 2007) of the method described by Ainsworth, Ferro-Famil, and Lee (2006). The forest area was used as a distributed target to estimate cross-talk parameters and cross-polarized channel imbalance while the co-polarized channels imbalance was estimated from six Passive Corner Reflectors (PCRs) deployed in a nearby homogeneous grassland field. Polarimetric calibrated data showed, over the PCRs, a mean ratio of the co-polarized channels of around 1 dB and a mean phase difference of 3° and 6° depending on the antenna. The absolute radiometric calibration coefficient was estimated as the difference between the backscattering coefficients obtained from PCRs and their theoretical radar cross-sections. After radiometric calibration, the difference between observed and theoretical PCR cross sections was an average of 0.9 dB with a standard deviation of 0.8 dB.

Table 1
Acquisition dates of the SAR data and the cumulative precipitation (three days prior to acquisition) recorded at the closest meteorological station (Narrandera airport — 10 km north). Rainfall (mm) recorded during the SAR acquisition day is provided in parentheses.

Sensor	Day1	Day2	Day3	Day4	Day5	Day6	Day7	Day8
PLIS	05.09.2011	07.09.2011	10.09.2011	13.09.2011	15.09.2011	19.09.2011	21.09.2011	23.09.2011
Rainfall (mm)	0.2 (0.2)	3.6 (3.4)	1.6 (1.6)	1.6 (0)	0 (0)	0 (0)	0 (0)	0 (0)

The SAR metrics derived from PLIS observations were divided into two groups. The first group corresponds to the backscatter intensity (BI) metrics which includes the intensity of the individual channels (i.e., HH, HV, VH and VV). The second group corresponds to backscattering components obtained through polarimetric target decomposition (TD). Pauli representation was used to separate the scattering matrix into simpler scattering responses related to single bouncing (HH + VV), double bouncing (HH − VV) and volume (2HV) scattering. By using incoherent polarimetric decompositions the coherency matrix was modeled as a function of three scattering mechanisms; surface scattering, double-bounce or dihedral scattering, and volume scattering (i.e., Freeman & Durden (1998), Yamaguchi et al. (2005), and van Zyl et al. (2011)). In addition, an eigenvector–eigenvalue decomposition was used to generate the entropy (H), anisotropy (A) and mean alpha angle (α) from the coherency matrix (Cloude & Pottier, 1997).

To reduce noise, backscatter intensities were estimated after multi-looking in range and azimuth by 2 and 14, respectively. The same factors were used to multi-look the coherency matrix. In addition, the coherency matrix was filtered using a 5 × 5 window (Lee, Grunes, Schuler, Pottier, & Ferro-Famil, 2006). The ground pixel spacing after multi-looking was around 10 m. All SAR metrics were geocoded to the Universal Transverse Mercator (UTM) coordinate system using a lookup table that described the transformation between the radar and the map geometries (Wegmüller, Werner, Strozzi, & Wiesmann, 2002). The lookup table was generated using a digital elevation model (DEM) and the flight information. To correct for possible inaccuracies in the input data, a refinement of the lookup table was applied, in the form of offsets between the PLIS images and a reference image mosaic derived from X-band SAR images provided by the Terrasar/Tandem-X mission. The geometric accuracy of the single look slant range complex data from the Terrasar satellite, and by extension of the co-registered Terrasar/TandemX product, was estimated to be better than 1 m (Fritz & Einder, 2010; Nonaka et al., 2008). High resolution representations of the backscatter intensity and van Zyl et al. (2011) target decomposition components are shown in Figure S2 and Figure S3 for the first day of the field campaign (5 September 2011).

3.2. Lidar data

Aircraft light detection and ranging (Lidar) acquisitions are useful for developing statistical or physically based models to spatially extend local measurements (Goetz & Dubayah, 2011). Lidar-based measurements were used to provide enough samples across variable forest structures to facilitate the development of remote sensing algorithms based on radar data. The full waveform-digitizing laser scanner Riegl Q560/240 kHz was flown over the forest area at an altitude of about 400 m at the beginning and the end of the SMAPEx3 campaign. The system, recording all echo pulses within a small footprint (~15 cm), was flown from two different directions (N–S and E–W) with a 50% swath overlap that resulted in the same area of the ground being covered four times. An average first return pulse density of 40 pulses per square meter (ppm) was obtained after combining all flight lines. The Riegl software package RiAnalyze was used to extract discrete returns from the raw lidar data. These returns were then combined with the navigation data to yield geo-referenced point clouds. Accuracies of data resulting from this procedure are approximately 0.4 m horizontally and 0.15 m vertically, with higher relative accuracies within individual scans. The point clouds were then classed into ground and non-ground returns with all non-ground returns being considered vegetation since no human-made features were located within the forest perimeter.

4. Methods

The study was structured in three parts. First the forest inventory and point cloud Lidar data were used to produce a reference biomass map. Second, backscatter intensities and polarimetric target decomposition components from multi-temporal airborne acquisitions were used to retrieve biomass through parametric and non-parametric modeling. Third, the influence of polarization and forest variability on biomass retrieval errors was investigated. The use of a reference Lidar based biomass map was necessary from two reasons: obtaining a representative number of samples for error analysis over the area covered by the airborne radar sensor (i.e., some field plots were outside the SAR swath — Fig. 1B and D panels) and obtaining plots of variable size centered at the same coordinates for studying the effect of plot size and forest variability on biomass estimation error. A flowchart (Fig. 3) is presented to make the methods used in this study clear. A straight up analysis of field biomass and L-band airborne data was carried out recently within a comparative study (Tanase et al., 2014). The study concluded that although Lidar data is overall twice as accurate when compared to L-band SAR data, for some biomass intervals SAR data could provide fundamentally similar results to Lidar when estimating forest biomass at high spatial resolution.

4.1. Lidar-based biomass reference map

Canopy height is an important forest attribute that can be used as a predictor variable for parameters such as biomass and forest volume (Lefsky et al., 2005; Nelson, Swift, & Krabill, 1988). However, lidar response to a forest canopy is not only a function of tree height, but also a function of canopy closure and density; the latter could be further used as a predictor of the forest structure and ultimately AGB (Arp, Griesbach, & Burns, 1982; MacLean & Krabill, 1986).

Multiple linear regression was used to produce a spatially continuous biomass map using lidar metrics and the field plots. Over 65 grid metrics were produced from lidar point cloud data at 5 m spatial resolution: i) canopy closure at 1, 2, 4, 6, 8, 10 and 12 m height, ii) canopy closure and forest density for specific strata (i.e., 1–4, 1–6,1–8, 1–10,1–12, 1–16, 1–24, 2–4, 2–6,…. 8–16, 8–24 m), and iii) overall metrics such as maximum height, canopy surface area and volume under the canopy surface. Canopy closure metrics were defined as the proportion of first returns over a specific height threshold. Strata specific canopy closure and forest density metrics were defined as the proportion of first returns and respectively all returns falling within specific height thresholds. The grid metrics were correlated with the ground-based plot information to select an appropriate subset for biomass prediction. The selected grid metrics were used to derive spatially explicit AGB estimates for the area covered by the lidar flight. Arcsine and log transformations were used to normalize the distribution of the lidar-based metrics and the plot-based biomass, respectively. Since cross-validated error magnitudes are far more valuable and indicative of true accuracy the regression parameterization was performed using 75% of randomly selected sample data, with the remaining 25% retained for validation (Goetz & Dubayah, 2011). The calibration process iterated the dataset

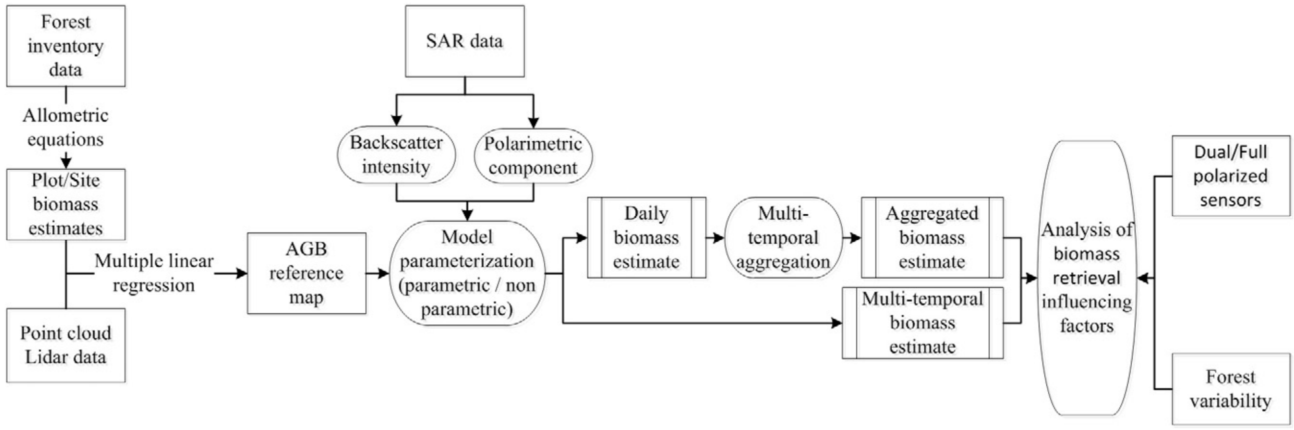

Fig. 3. Flowchart of biomass retrieval from SAR data.

10 times with the dataset being randomly split into training and validation subsets to allow a robust estimation of the error of the AGB reference map.

4.2. SAR based estimation of biomass from multi-temporal L-band data

Biomass estimation was undertaken by decomposing the PLIS polarimetric data into surface, double bounce and volume contributions and subsequently using the metrics obtained within parametric and non-parametric models. Although recent studies (Mitchard et al., 2009; Sandberg et al., 2011) showed that models based on multiple polarizations (i.e., HH, HV, VV) do not significantly improve biomass estimation accuracy, it was decided to corroborate these results for a significantly different environment characterized by relatively short trees and low biomass levels. Previously, several models were investigated for the retrieval of biomass from space borne L-band SAR data, starting from simple regression based parametric models to semi-empirical water cloud-like models or non-parametric models (Tanase et al., in press). Since similar model types provided comparable results it was decided to present only one model in each category (i.e., parametric and non-parametric). The parametric models selected for biomass retrieval (Eqs. 1 and 2) were modified from the Sandberg et al. (2011) model by allowing for the effect of the incidence angle variation from near- to far-range to be considered in the estimation. In this study, the average incidence angle at each sample plot was included as a predictor variable.

$$\sqrt{AGB} = a_0 + a_1 * SARm_1 + a_2 * \cos\theta \quad (1)$$

$$\sqrt{AGB} = a_0 + a_1 * SARm_1 + a_2 * SARm_2 + a_3 * SARm_3 + a_4 * \cos\theta \quad (2)$$

where:

AGB–aboveground biomass $\left(\mathrm{Mg\ ha^{-1}}\right)$

$a_0 a_1 a_2 a_3 a_4$–unknown model coefficients

$SARm_x$–SAR BI or TD metric (logarithmic scale)

θ–average local incidence angle at the sample plot.

The non-parametric model selected to estimate AGB levels was the random forest (RF). Up to three SAR metrics (e.g., HH, HH and HV, surface, and dihedral and volume scattering) and the incidence angle were executed in the RF model to retrieve biomass. RF regression (Breiman, 2001) uses ensemble learning methods by constructing a large number of decision trees from the training data which are subsequently used to derive overall predictions as the average response from all individually trained trees.

After model parameterization and inversion, daily AGB estimates become available for each validation sample and radar metric. Such daily estimates were viewed as different attempts to “guess” the biomass level. Without a priori information it is impossible to determine which of these “guess” estimates are closest to the real biomass levels. However, by aggregating daily AGB estimates one could decrease the uncertainty in biomass estimation associated with the daily values. Several methods were used to combine the daily biomass estimates by SAR metric: i) simple averaging (Da), ii) averaging only the values within 1.5 standard deviations of the local mean and iii) weighted average with more weight being given to the dates showing higher dynamic range from bare soil to dense forest. Since all of these aggregation methods provided very similar values, only the results obtained for the simple averaging (Da) are presented in the following sections. The aggregation of all daily biomass estimates obtained from the BI or TD metrics was also used to obtain a final AGB value. The method involved averaging the biomass estimates obtained for all days and all SAR metrics (Da-all) by metric type.

Biomass estimates based on multi-temporal (MT) data were obtained by i) simultaneously using all daily backscatter values for a given SAR metric when parameterizing the RF model (MT-all) and by ii) averaging daily backscatter into one unique multi-temporal value, by SAR metric, followed by the parameterization of the various models (MT-ma). The coefficient of determination (R^2), the root mean squared error (RMSE) and the relative RMSE (ratio between RMSE and mean biomass — RMSE%) were used to assess which SAR metric and aggregation method are best suited for biomass retrieval.

4.3. Factors that influence biomass retrieval

Two factors influencing biomass retrieval from SAR system were investigated in this study: available polarizations and the mapping unit area. Biomass estimation from fully polarimetric and dual polarized data was evaluated by using BI metrics and the RMSE% was compared. The RMSE% was computed after averaging all daily biomass estimates (Da-all) obtained from single parametric model inversion for the two or four polarizations. In addition, the benefit of a full polarization sensor was further inferred by comparing the R^2, RMSE, and RMSE% obtained for BI and TD metrics.

Random plots at various radii were used to assess the effects of mapping unit area to the AGB retrieval accuracy. For forest biophysical characteristic retrieval from radar data the selection of an appropriate estimation scale has major impacts related to decreasing radar speckle with increasing area and decreasing forest heterogeneity. Such effects result in better estimations of the backscatter values and smaller forest variability. SAR backscatter metrics and lidar-based biomass were extracted at corresponding locations using 10, 15, 25, 50, 75, and 100 m radius plots, which are equal to 0.003, 0.07, 0.2, 0.8, 1.8, and 3.1 ha, respectively. The RMSE% was related to forest variability expressed by the coefficient of variation for each plot size. RMSE% was computed by averaging all daily biomass estimates obtained from single parametric model inversion (i.e., Da-all aggregation method).

5. Results

5.1. Biomass reference map

For each forest stratum one lidar metric was retained to derive the biomass reference map (Fig. 1 panel E and Figure S1): the pulse density of the 1–12 m height stratum (D_{1-12}) was selected to describe the dense understory layer while for the overstory layer the canopy percent cover in the 6–8 m height stratum (C_{6-8}) was retained. As a general descriptor of the plot structure the volume under the forest canopy surface was used (C_{vol}). This metric had the highest correlation with all biomass components and was always included as a predictor variable by a stepwise regression analysis. At plot level, the error of the lidar-based biomass reference map was estimated as 17.2 Mg ha^{-1} for average biomass levels of 60 Mg ha^{-1}. When analyzed at the site level the error decreased to 13.2 Mg ha^{-1}. This decrease was explained by the lower forest variability at such spatial scales, the higher confidence in the ground measured biomass aggregates, and the reduced effect of the plot positioning errors.

5.2. SAR based estimation of biomass from multi-temporal L-band data

Although several parametric and non-parametric models were evaluated for biomass retrieval only results obtained for models (1), (2) and RF are presented (Tables 2 and 3). Similarly, only results obtained for the van Zyl et al. (2011) polarimetric target decomposition method are presented since it provided the highest biomass retrieval accuracy when compared to the remaining decomposition models (i.e., Freeman–Durden, Yamaguchi and Cloude–Pottier) or the Pauli basis representation. A total of 131 random sample plots were used to extract co-located lidar based AGB estimates and SAR BI and TD metrics for model parameterization/validation. At 15 m radius the reference AGB for the selected random plots varied between 2.0 and 156.0 Mg ha^{-1} with over 93% of them being below 100 Mg ha^{-1}. The mean plot biomass was 47.8 Mg ha^{-1} with a standard deviation of $\pm$29.8 Mg ha^{-1}. At 100 m radius the maximum AGB was 120.2 Mg ha^{-1}. The mean plot biomass was 50.0 Mg ha^{-1} with a standard deviation of $\pm$22.2 Mg ha^{-1}. Depending on the flight day the estimated AGB ranged from 0.2 to 103.1 Mg ha^{-1} with a mean value of 46.0 Mg ha^{-1} when using the fully polarized parametric model within single date retrieval for 15 m radius plots. For multi-temporal retrieval through aggregation (i.e., Da) the estimated AGB ranged from 0.71 Mg ha^{-1} to 88.2 Mg ha^{-1}. The daily temporal change of the retrieved biomass for three typical plots is shown in Fig. 4.

For BI metrics Table 2 shows that daily RMSE% can fluctuate up to 10% depending on metric selection and modeling approach. The lowest daily difference, 2 to 4%, was observed for parametric models. Single metric models showed roughly similar estimation errors while a marginal improvement of up to 2% was observed for the model containing multiple polarizations. When using non-parametric models the selection of the SAR metric played a more important role, with the maximum daily variation of the RMSE% reaching 5 to 10%. In addition, a model including multiple polarizations did not improve the estimation accuracy on a consistent basis. Similar results were observed for TD metrics (Table 3). The main difference with respect to BI metrics was the larger overall fluctuation, up to 15%, and the smaller difference, up to 1.5%, between models containing one or several target decomposition metrics. Generally, TD metrics that related to volume scattering mechanisms provided better results with higher R^2 and lower RMSE and RMSE% being observed when compared to using metrics related to dihedral and surface scattering. When comparing BI and TD metrics results showed that BI metrics were generally more accurate when using parametric models, and less accurate when using non-parametric models. The aggregation of the daily biomass estimates did not improve the retrieval

Table 2
Indicators of biomass retrieval accuracy from backscatter intensity (BI) metrics (0.07 ha plots). Da and Da-all refer to different aggregation methods of daily biomass estimates (see Section 4.3). Multi-temporal (MT) refers to calibration of models using the average of the daily SAR metrics (MT-ma) while MT-all refers to calibration of random forest (RF) models by simultaneously using all daily values for a given SAR metric.

Model	SAR metric	Daily models and multi temporal averages of biomass estimates										MT-ma
		Day1	Day2	Day3	Day4	Day5	Day6	Day7	Day8	Da	Da-all	
						R^2						
(1)	HH	0.591	0.536	0.573	0.554	0.558	0.565	0.557	0.596	N/A		0.588
	HV	0.542	0.529	0.528	0.524	0.537	0.535	0.568	0.577		N/A	0.567
	VV	0.534	0.447	0.548	0.530	0.529	0.496	0.578	0.543			0.560
(2)	HH, HV, VV	0.610	0.589	0.608	0.595	0.597	0.586	0.623	0.625			0.621
						RMSE (Mg ha^{-1})						
(1)	HH	21.2	22.7	22.2	22.5	22.4	22.3	22.6	21.1	21.8	21.5	21.7
	HV	22.9	22.7	23.1	23.2	22.8	23.0	22.2	21.7	22.3		22.3
	VV	22.9	22.5	23.2	23.1	22.8	23.1	22.1	21.7	22.3		21.9
(2)	HH, HV, VV	21.1	21.6	21.3	21.8	21.6	22.0	21.1	20.7	21.1	N/A	21.1
						RMSE%						
(1)	HH	44.4	47.6	46.4	47.0	46.8	46.7	47.3	44.2	45.5	45.1	45.3
	HV	47.8	47.5	48.4	48.5	47.8	48.2	46.5	45.5	46.8		46.7
	VV	48.0	47.1	48.6	48.5	47.7	48.5	46.3	45.5	46.7		45.8
(2)	HH, HV, VV	44.2	45.3	44.7	45.6	45.2	46.1	44.2	43.4	44.2	N/A	44.1
						Non-parametric RMSE%						
Daily models											MT-all	MT-ma
RF	HH	47.6	55.0	54.4	55.4	54.6	53.0	55.0	51.9		44.3	50.5
	HV	49.6	50.5	49.4	51.1	51.9	49.3	47.8	46.0	N/A	48.1	48.9
	VV	46.3	48.7	48.4	46.8	47.0	48.3	44.6	49.3		45.8	45.0
	HH, HV, VV	42.5	49.0	47.3	49.2	47.7	48.5	46.4	44.3		N/A	40.0

Table 3
Indicators of biomass retrieval accuracy from target decomposition (TD) metrics (van Zyl et al. (2011) decomposition, 0.07 ha plots). Da and Da-all refer to different aggregation methods of daily biomass estimates (see Section 4.3). Multi-temporal (MT) refers to calibration of models using the average of the daily SAR metrics (MT-ma) while MT-all refers to calibration of random forest (RF) models by simultaneously using all daily values for a given SAR metric.

Model	SAR metric	Daily models and multi temporal averages of biomass estimates										MT-ma
		Day1	Day2	Day3	Day4	Day5	Day6	Day7	Day8	Da	Da-all	
						R^2						
(1)	Surface (S)	0.473	0.350	0.386	0.391	0.461	0.445	0.471	0.481	N/A		0.485
	Double (D)	0.411	0.424	0.512	0.486	0.454	0.456	0.494	0.445		N/A	0.470
	Volume (V)	0.518	0.500	0.506	0.521	0.504	0.496	0.509	0.519			0.514
(2)	S, D, V	0.556	0.526	0.550	0.543	0.547	0.546	0.555	0.568			0.551
						RMSE ($Mg\ ha^{-1}$)						
(1)	Surface (S)	23.0	25.3	24.9	24.9	23.3	23.5	23.6	22.8	23.0	22.7	23.2
	Double (D)	24.9	24.5	23.2	23.5	24.5	24.4	23.8	24.5	23.7		24.0
	Volume (V)	23.3	23.4	23.6	23.3	23.6	23.9	23.5	23.2	23.4		23.4
(2)	S, D, V	22.3	23.0	22.7	22.8	22.6	22.6	22.6	22.1	22.4	N/A	22.6
						RMSE%						
(1)	Surface (S)	48.2	52.9	52.2	52.1	48.7	49.1	49.3	47.7	48.2	47.5	48.6
	Double (D)	52.2	51.4	48.5	49.2	51.4	51.2	49.8	51.2	49.6		50.3
	Volume (V)	48.8	49.0	49.4	48.8	49.3	50.0	49.3	48.6	49.0		48.9
(2)	S, D, V	46.7	48.2	47.4	47.8	47.3	47.4	47.3	46.2	46.9	N/A	47.3
						Non-parametric RMSE%						
Daily models											MT-all	MT-ma
RF	Odd (O)	49.2	53.3	52.4	50.5	49.6	52.4	48.3	50.5		50.6	51.6
	Double (D)	57.0	57.4	51.0	56.3	58.8	55.4	52.0	58.1	N/A	53.6	54.2
	Volume (V)	47.2	45.7	47.2	47.0	48.2	47.8	45.3	46.8		50.4	48.2
	O, D, V	43.6	46.2	44.3	45.8	44.0	46.4	43.1	44.2		N/A	44.9

accuracy. However, it did provide more reliable estimates since the overall RMSE% of the biomass aggregates were close to the lowest daily RMSE%. Finally, models based on multi-temporal data (i.e., MT-all and MT-ma) did not improve the biomass estimation accuracy significantly, with RMSE% being close to the values obtained for some of the most accurate daily models.

5.3. Factors that influence biomass retrieval

The difference in relative error (Da-all aggregation method) when using PLIS full polarized data as compared to only using two polarizations (i.e., HH and HV) is shown in Fig. 5. The errors are shown for plot sizes corresponding to the different extraction radii used. AGB estimation accuracy increased up to 0.5% when using full polarized data especially for smaller plots. With increasing plot size the difference in AGB estimation error decreases with dual polarized data reaching the same accuracy as fully polarized data for the 0.8 ha plot size.

The influence of the pixel size on the modeled relationships between HV polarization and AGB is shown in Fig. 6 while the relationship between the relative retrieval error and forest variability for different plot sizes is shown in Fig. 7. Forest variability was expressed by the coefficient of variation (CV) of the reference AGB. A significant influence of the plot size was observed for all models and SAR metrics with the estimation error decreasing according to increasing plot size. Depending on the plot size, SAR metric, day and aggregation method the decrease varied between 10% and 30%. A very strong correlation ($R^2 = 0.95$, $p < 0.001$) between the AGB estimation error and forest variability was also observed (Fig. 6).

6. Discussion

Previous studies have shown biomass estimation errors from SAR data to be around 45 to 80% with respect to the reference values (Harrell et al., 1997; Rignot, Way, Williams, & Viereck, 1994; Sandberg et al., 2011). With the exclusion of older stands or the selection of more homogeneous ones the estimation errors have been as low as 25% to 40% (Rignot et al., 1994; Santoro et al., 2006). This study has shown that AGB estimation errors can vary between 30% and 50% in semi-arid areas depending on the spatial resolution at which the estimates are needed. For relatively high spatial resolutions (i.e., 25 m) biomass estimation error reached 45% when using backscatter intensity metrics, and increased by another 2–3%, when using polarimetric target

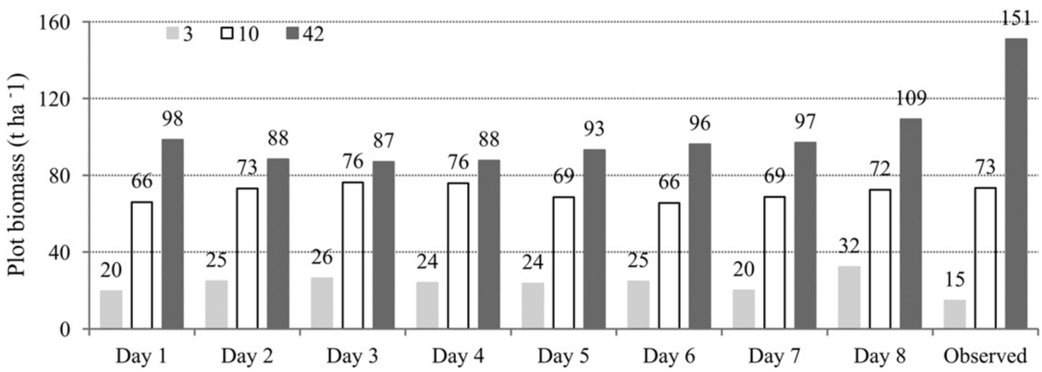

Fig. 4. Daily temporal changes in biomass retrieval for three representative plots (3, 10 and 42) spanning the entire biomass range.

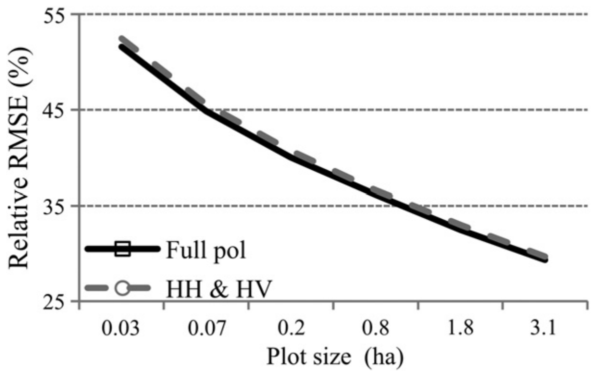

Fig. 5. AGB relative retrieval error (RMSE%) when using full and dual polarized PLIS data.

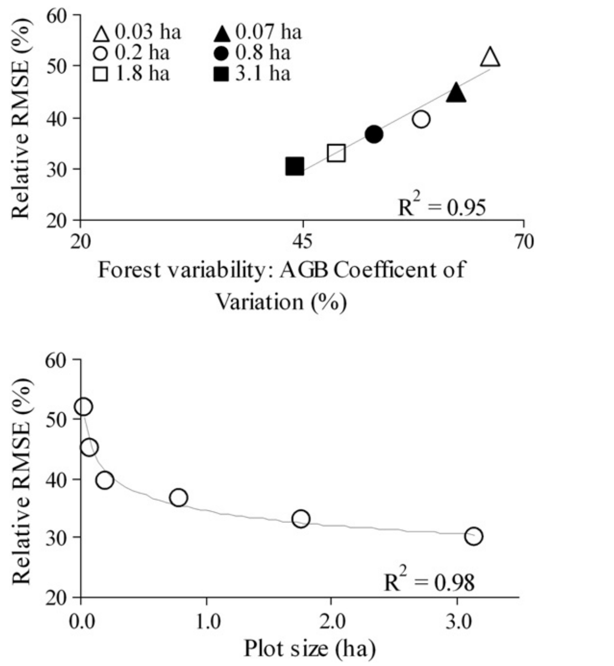

Fig. 7. Relationship between relative retrieval error and forest variability (top). Observed decline in biomass prediction error with decreasing spatial resolution (bottom).

decomposition components or their linear combinations (e.g., ratio between volume and surface scattering). The analysis showed that, in semi-arid areas, retrieval accuracy of forest biomass from L-band radar backscatter observations is relatively stable, within 10%, for images acquired at short intervals and depends little on the selected SAR metric (i.e., BI or TD) or modeling approach (i.e., parametric or non-parametric). It is noted that during the airborne PLIS acquisitions moderate changes in soil moisture and canopy water content were observed, with soil moisture decreasing by an average 7% and the leaf water content decreasing by an average 30%. However, such changes were not systematically related to changes in biomass retrieval (Table 1 and Fig. 4).

Neither the aggregation of daily biomass estimates nor the use of multi-temporal based models improved the retrieval accuracy beyond the most accurate daily estimate for a given metric. However, a priori knowledge of the true biomass value is not usually available since it is the quantity being estimated. By using aggregation methods of multi-temporal data the average estimation error with respect to the worst daily estimate improved by up to 5%. In addition, for 45% of the samples the daily estimates presented higher errors when compared to the error recorded for the aggregated value. Therefore, multi-temporal data has the potential to provide more reliable values with respect to single-date approaches. This could be especially valid when variations of the environmental conditions are large, which was not the case in the current study.

Contrary to other studies (Harrell et al., 1997; Le Toan et al., 1992; Rignot et al., 1994; Sandberg et al., 2011) slightly lower errors, 1–2% less, were obtained for the co-polarized channels as compared to the cross-polarized channels. This could be attributed to the specific forest structure of this study area, which is characterized by a relatively low height overstory layer and large gaps among tall trees. Such forest structures coupled with the long L-band wavelength allow for greater canopy penetration by microwaves and thus more interactions with the ground surface, to which the co-polarized channels are more sensitive.

Other studies (Sandberg et al., 2011) have shown that there is little to be gained when simultaneously using co- and cross-polarized channels within a common model. The results of this study confirm such findings in semi-arid environments, not only for parametric but also for non-parametric modeling approaches. An average improvement of 3% in biomass retrieval accuracy, as observed by this study, provides little incentive for acquiring fully polarized SAR datasets which usually come at the expense of spatial resolution or coverage. Furthermore, model parameterization using polarimetric target decomposition metrics obtained from fully-polarimetric data did not result in improved biomass estimation accuracies for our study area. Special attention was given to polarimetric target decomposition metrics since both of the near-term L-band missions (i.e., ALOS PALSAR-2 and SAOCOM), will feature fully polarized sensors. The sensitivity to biomass level was comparable between TD and BI metrics. Although produced for a different environment and forest type, the results of the present study confirm the findings in Neumann et al. (2012), which state that L-band data produce better correlations with AGB from backscatter intensities than PolSAR-derived metrics. However, it is noted that no attempt was made to use more advanced techniques such as polarimetric

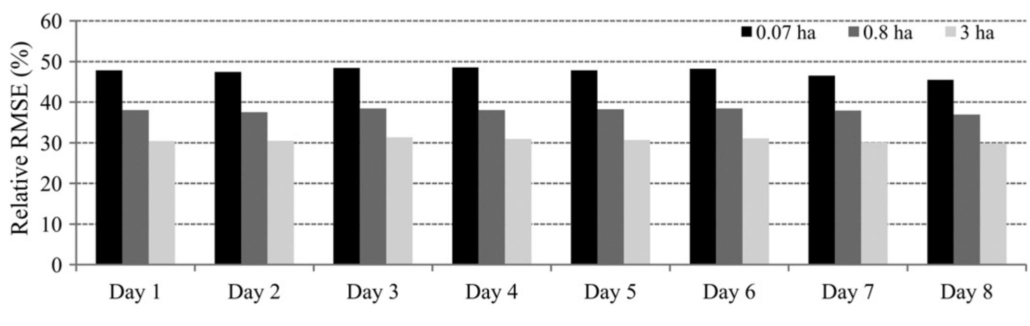

Fig. 6. Influence of plot size on AGB estimation error for HV polarized PLIS data.

interferometry. For L-band SAR data, polarimetric interferometry might provide better results when combined with BI and/or TD metrics (Neumann et al., 2012).

It is well know that errors tend to decline with increasing plot size (Frazer, Magnussen, Wulder, & Niemann, 2011; Mascaro, Detto, Asner, & Muller-Landau, 2011; Zolkos, Goetz, & Dubayah, 2013). Spatial averaging of the errors might contribute to this observation (Goetz & Dubayah, 2011). However, this study shows that such observations are related to forest heterogeneity. With increasing plot size, forest variability decreases which directly translates into lower estimation errors. Therefore, a general rule of thumb regarding the optimum plot sampling size is far from straightforward since for highly homogeneous forest such as plantations small plot sizes could be sufficient to capture the entire forest structural variability. For remote sensing missions a 20% error is commonly employed as an objective (Zolkos et al., 2013). Such an objective could be reached using radar backscatter-based modeling when forest variability decreases below 40%. However, for such high accuracy to be achieved the sampling effort could become substantial in highly heterogeneous forests.

Previous studies have demonstrated that at very coarse spatial resolutions (i.e., 1 to 10 km) the estimation errors could reach 20–25% (Saatchi, Houghton, Dos Santos, Soares, & Yu, 2007; Santoro et al., 2011). Such accuracies are most probably related to the significant reduction in forest variability expected at such spatial scales. The improvement of goodness-of-fit/evaluative statistics associated with coarser spatial resolution must be interpreted cautiously, however. There is an extensive body of literature on the modifiable area unit problem (MAUP) that arises when analysis is undertaken at multiple spatial resolutions (Holt, Steel, Tranmer, & Wrigley, 1996; Openshaw, 1984; Unwin, 1996). Correlations among spatial phenomena regularly improve as pixel size increases. As noted, this is partly related to the decrease in variability caused by averaging. It can also be related, however, to a decrease in the number of observations such as occurs when 100 “small” pixels are compressed into 10 “big” pixels, although this is less important if the number of big pixels remains large ($n = 50+$). Because of the MAUP, interpretation of analytical results must be constrained to the pixel size used in the analysis.

The results of this study show that substantial improvements of the retrieval accuracy are possible at much higher spatial resolutions (i.e., 150–200 m) by reducing the uncertainty of the reference biomass estimates, the SAR metrics' signal-to-noise ratio, and the possible co-registration errors among datasets. Such enhancements were possible by decreasing the spatial resolution of the input datasets which is equivalent to increasing the radius of the plots used for data extraction from both the lidar-based reference map and the geocoded SAR metrics. Thus, by increasing the plot size to approximately 3 ha (i.e., 175 m pixels) the forest variability decreases by approximately 20% in our study area, which in turn facilitated a more accurate AGB estimation, although the resulting estimates are only applicable to larger areas — i.e., at the coarser spatial resolution as noted above. At such pixel size the biomass estimation error decreased to 30% from the more than 50% recorded for 20 m pixels.

Relatively few studies (Robinson et al., 2013; Saatchi et al., 2011) have tried to assess forest variability and its effects on biomass retrieval using radar data. Although both studies observed a decrease in RMSE with increasing plot size they were somewhat limited by the low number of samples available within the sensitivity-to-biomass interval of L-band. Saatchi et al. (2011) ascribed the decrease in RMSE to speckle noise reduction and reduced geolocation errors. Although speckle and geolocation errors might affect the biomass/backscatter relationship, we have shown that while speckle noise is relatively low (i.e., 42 looks for 10 m radius plots of PLIS data) the RMSE is still substantial. Robinson et al. (2013) recognized that the sensitivity to AGB may improve at large spatial scales when effects of forest structure are averaged out. This was demonstrated by the current study which has shown that even fine resolution SAR imagery contains considerable noise which was mainly caused by inherent forest structural variability: 95% of the RMSE errors encountered for decreasing plot size were explained by forest variability. Such noise can be eliminated by decreasing the variability related to the sampling plots when products at lower spatial resolutions are sufficient. However, high spatial resolution products sometimes are necessary, especially for highly fragmented forest areas. Users of such research results must be aware of the trade-off between a stronger relationship that is only applicable for large pixels (i.e., increased R^2 and decreased errors for larger mapping area), or a weaker relationship and higher errors at a more spatially explicit scale.

In studies such as the present one, field data are commonly recorded for relatively small plots (<1 ha) due to labor costs and time constraints. Although not an objective, this paper demonstrated the value of having local reference AGB estimates at the scale of observation required. In this study such estimates were obtained from lidar data. The availability of lidar-based local AGB estimates assisted the retrieval algorithms, providing sufficient data for both model parameterization and validation at different spatial resolutions. The recent dismissal of NASA's Deformation, Ecosystem Structure and Dynamics of Ice (DESDynI) lidar mission means that high quality lidar-based AGB estimates will not be available for future SAR missions. This will hinder large-scale biomass retrieval since models calibrated with local data could provide better retrieval accuracies than more universal models.

7. Conclusions

This paper studied the potential of upcoming L-band SAR missions to improve forest biomass retrieval accuracy in semi-arid environments. Multi-temporal SAR data were acquired every two to three days over three weeks using an airborne fully polarized L-band sensor. Parametric and non-parametric models were calibrated to retrieve AGB from backscatter intensities and polarimetric target decomposition metrics within single and multi-date retrieval approaches.

The most reliable biomass estimates were obtained when using multi-temporal data. However, the multi-temporal biomass estimates did not improve the retrieval accuracy beyond the most accurate daily estimate. Fully polarized systems improved biomass estimation accuracy only marginally over dual-polarized systems when using backscatter intensity metrics. Polarimetric target decomposition-based retrieval showed similar sensitivity to biomass levels as when using backscatter intensities. Overall, parametric models performed slightly better for both single and multi-metric retrieval. The most significant improvement in biomass retrieval accuracy was achieved by reducing the spatial resolution at which the estimates were produced. At lower spatial resolutions the forest spatial variability reduces allowing for decreasing the estimation error to up to 30%. The 1:1 relationship between forest variability and biomass estimation error has considerable implications since even high spatial resolution sensors would not be sufficient to produce very accurate biomass maps at fine scales (i.e., 10 or 20 m pixel size).

Acknowledgments

The authors wish to thank Alvin Goh and Mark Williams for assisting with the PLIS calibration, Andrew McGrath and Wolfgang Lieff for undertaking the Lidar flights and the SMAPEx experiment participants for support with field data collection. The German Aerospace Center (DLR) is acknowledged for providing the TerraSAR/TanDEM-X data (project XTI VEGE0896). The study was conducted under an Australian Research Council (ARC) Super Science Fellowship (FS100100040). The field work was supported by the Cooperative Research Centre for Spatial Information and the ARC Discovery Project DP0984586.

Appendix A

Table A1
Field plot data used for the estimation of the biomass reference map. Species proportion is rounded to the nearest multiple of five. Mean trees dbh and height are computed only using trees not saplings. Saplings refer to trees with dbh below 5 cm. Above ground biomass (AGB) refers to the sum of trees, saplings and grass biomass. The center coordinates of the Gillenbah forest are 146.50° E, 34.81° S.

Site	Plot	Present species and their proportion (%)	Mean tree dbh (cm)	Mean tree height (m)	Number of trees	Number of saplings	Total AGB (Mg ha^{-1})
1	c	Ca (100)	42.6	14.9	5	0	69.5
1	e	Ca (90) Pi (10)	14.2	9.6	33	0	75.8
1	n	Ca (80) Eu (20)	20.6	10.7	14	0	74.2
1	s	Ca (90) Pi (10)	17.6	8.7	16	0	50.5
1	w	Ca (30) Eu (55) Pi (15)	42.4	18.3	7	0	143.8
10	c	Ca (75) Eu (25)	18.1	8.7	34	0	176.9
10	e	Ca (75) Eu (25)	15.6	8.5	15	430	52.7
10	n	Ca (80) Eu (20)	11.8	6.0	34	213	167.3
10	s	Ca (50) Eu (50)	10.7	7.4	10	354	24.1
10	w	Ca (95) Eu (5)	12.2	6.4	24	66	129.1
15	c	Ca (100)	14.9	8.5	23	28	70.8
15	e	Ca (100)	7.3	5.6	80	96	32.4
15	n	Ca (100)	20.6	9.9	18	111	86.0
15	s	Ca (100)	17.8	9.7	14	63	57.0
15	w	Ca (100)	8.4	5.7	44	115	55.3
17	c	Ca (90) Eu (10)	12.1	6.4	40	83	179.5
17	e	Ca (80) Eu (20)	12.5	6.7	34	0	55.0
17	n	Ca (100)	9.4	6.0	49	72	42.8
17	s	Ca (100)	9.5	6.1	47	29	39.1
17	w	Ca (100)	9.3	5.6	40	0	46.4
20	c	Ca (100)	7.3	4.9	47	21	18.3
20	e	Ca (95) Eu (5)	8.7	5.5	51	60	32.5
20	n	Ca (100)	9.2	6.0	65	72	50.6
20	s	Ca (100)	12.5	6.8	32	0	42.3
20	w	Ca (100)	9.0	5.8	65	88	53.7
23	c	Ca (100)	11.0	6.5	21	70	34.7
23	e	Ca (100)	7.3	5.5	93	99	36.8
23	n	Ca (100)	7.3	5.6	103	151	45.0
23	s	Ca (100)	15.0	6.3	9	30	16.4
23	w	Ca (100)	12.5	6.8	23	0	34.4
24	c	Ca (100)	10.6	6.7	55	0	47.8
24	e	Ca (100)	11.0	6.8	30	15	40.2
24	n	Ca (100)	13.4	7.5	36	0	55.9
24	s	Ca (100)	8.2	5.6	75	41	44.5
24	w	Ca (95) Eu (5)	13.5	7.7	30	2	52.2
30	c	Ca (100)	8.5	4.7	40	140	38.8
30	e	Ca (100)	8.2	5.4	67	165	41.0
30	n	Ca (100)	7.2	4.7	43	550	44.6
30	s	Ca (100)	9.1	5.2	42	165	44.2
30	w	Ca (100)	7.6	4.5	48	121	32.7
38	c	Ca (100)	13.6	7.5	37	80	62.1
38	e	Ca (100)	16.2	8.1	17	0	39.8
38	n	Ca (100)	13.2	7.3	24	0	39.3
38	s	Ca (100)	8.7	5.8	62	63	52.3
38	w	Ca (100)	8.0	5.1	57	45	36.7
42	c	Ca (100)	6.8	5.0	68	38	22.2
42	e	Ca (100)	8.7	5.5	53	86	43.9
42	n	Ca (100)	7.1	4.9	51	68	25.8
42	s	Ca (100)	7.2	5.2	53	163	24.6
42	w	Ca (100)	6.8	4.9	36	420	27.9
67	c	Ca (100)	16.2	9.7	33	0	75.8
67	e	Ca (100)	17.5	8.8	23	10	76.5
67	n	Ca (100)	10.2	6.0	47	99	49.6
67	s	Ca (100)	9.9	6.4	53	26	36.9
67	w	Ca (100)	11.1	6.8	43	56	59.1
99	c	Ca (85) Eu (15)	15.5	9.6	37	47	143.1
99	e	Ca (90) Eu (10)	15.6	9.2	29	55	87.7
99	n	Ca (70) Eu (30)	22.0	11.6	24	61	152.1
99	s	Ca (100)	12.1	7.8	49	20	56.4
99	w	Ca (100)	13.8	7.1	19	30	35.8

Appendix B. Supplementary data

Supplementary data to this article can be found online at http://dx.doi.org/10.1016/j.rse.2014.01.024.

References

Ainsworth, T. L., Ferro-Famil, L., & Lee, J. S. (2006). Orientation angle preserving a posteriori polarimetric SAR calibration. *IEEE Transactions on Geoscience and Remote Sensing*, *44*, 994–1003.

Arp, H., Griesbach, J., & Burns, J. (1982). Mapping in tropical forests: A new approach using the laser APR. *Photogrammetric Engineering & Remote Sensing*, *48*, 91–100.
Attema, E. P. W., & Ulaby, F. T. (1978). Vegetation modeled as a water cloud. *Radio Science*, *13*, 357–364.
Breiman, L. (2001). Random forests. *Machine Learning*, *45*, 5–32.
Burgin, M., Clewley, D., Lucas, R., & Moghaddam, M. (2011). A generalized radar backscattering model based on wave theory for multilayer multispecies vegetation. *IEEE Transactions on Geoscience and Remote Sensing*, *49*, 4832–4845.
Burrows, W. H., Hoffman, M. B., Compton, J. F., & Back, P. V. (2001). Allometric relationships and community biomass stocks in White Cypress Pine (*Callitris glaucophylla*) and associated eucalypts of the Carnarvon area, central Queensland. In N.C.A.S. (NCAS) (Ed.), *Technical Report*, *33*.
Cloude, S. R. (2006). Polarization coherence tomography. *Radio Science*, *41*, 1–27.
Cloude, S. R. (2007). Dual-baseline coherence tomography. *IEEE Transactions on Geoscience and Remote Sensing Letters*, *4*, 127–131.
Cloude, S. R., & Papathanassiou, K. P. (1998). Polarimetric SAR interferometry. *IEEE Transactions on Geoscience and Remote Sensing*, *36*, 1551–1565.
Cloude, S. R., & Pottier, E. (1996). A review of target decomposition theorems in radar polarimetry. *IEEE Transactions on Geoscience and Remote Sensing*, *34*, 498–518.
Cloude, S. R., & Pottier, E. (1997). An entropy based classification scheme for land applications of polarimetric SAR. *IEEE Transactions on Geoscience and Remote Sensing*, *35*, 68–78.
Cronin, N. L. R. (2004). *The potential of airborne polarimetric synthetic aperture radar data for quantifying and mapping the biomass and structural diversity of woodlands in semiarid Australia*. School of Biological, Earth and Environmental Sciences. Sydney: The University of New South Wales, 517.
Curlander, J., Holt, B., & Hussey, K. (1985). Determination of sea ice motion using digital SAR imagery. *IEEE Journal of Oceanic Engineering*, *10*, 358–367.
Dobson, M. C., Pierce, L., Sarabandi, K., Ulaby, F. T., & Sharik, T. (1992). Preliminary analysis of ERS-1 SAR for forest ecosystem studies. *IEEE Transactions on Geoscience and Remote Sensing*, *30*, 203–211.
Dobson, M. C., Ulaby, T., Le Toan, T., Beaudoin, A., & Kasischke, E. S. (1992). Dependence of radar backscatter on coniferous forest biomass. *IEEE Transactions on Geoscience and Remote Sensing*, *30*, 412–415.
Dong, Y., Milne, A. K., & Forster, B. C. (2001). Segmentation and classification of vegetated areas using polarimetric SAR image data. *IEEE Transactions on Geoscience and Remote Sensing*, *39*, 321–329.
Eldhuset, K. (1996). An automatic ship and ship wake detection system for spaceborne SAR images in coastal regions. *IEEE Transactions on Geoscience and Remote Sensing*, *34*, 1010–1019.
Englhart, S., Keuck, V., & Siegert, F. (2011). Aboveground biomass retrieval in tropical forests — The potential of combined X- and L-band SAR data use. *Remote Sensing of Environment*, *115*, 1260–1271.
Frazer, G. W., Magnussen, S., Wulder, M.A., & Niemann, K. O. (2011). Simulated impact of sample plot size and co-registration error on the accuracy and uncertainty of LiDAR-derived estimates of forest stand biomass. *Remote Sensing of Environment*, *115*, 636–649.
Freeman, A., & Durden, S. L. (1998). A three-component scattering model for polarimetric SAR data. *IEEE Transactions on Geoscience and Remote Sensing*, *36*, 963–973.
Fritz, T., & Einder, M. (2010). TerraSAR-X ground segment, basic product specification documentIn C. A.R. Sensing (Ed.).
Garestier, F., Dubois-Fernandez, P. C., & Papathanassiou, K. P. (2008). Pine forest height inversion using single-pass X-Band PolInSAR data. *IEEE Transactions on Geoscience and Remote Sensing*, *46*, 59–68.
Gibbs, H. K., Brown, S., Niles, J. O., & Foley, J. A. (2007). Monitoring and estimating tropical forest carbon stocks: Making REDD a reality. *Environmental Research Letters*, *2*, 1–13.
Goetz, S., & Dubayah, R. (2011). Advances in remote sensing technology and implications for measuring and monitoring forest carbon stocks and change. *Carbon Management*, *2*, 231–244.
Goh, A. S., Preiss, M., Gray, D. A., & Stacy, N. J. S. (2007). Comparison of parameter estimation accuracy of distributed-target polarimetric calibration techniques. *Geoscience and remote sensing symposium, 2007. IGARSS '07. Proceedings. 2007 IEEE International* (pp. 4175–4178).
Gonçalves, F. G., Santos, J. R., & Treuhaft, R. N. (2011). Stem volume of tropical forests from polarimetric radar. *International Journal of Remote Sensing*, *32*, 503–522.
Gray, D., Ruiting, Y., Yardley, H., Panciera, R., Walker, J., Hacker, J., McGrath, A., Bates, B., & Stacy, N. (2011). PLIS: An airborne polarimetric L-band interferometric synthetic aperture radar. *Synthetic Aperture Radar (APSAR), 2011 3rd International Asia-Pacific Conference on (pp. 1–4). Seoul.*
Hajnsek, I., Kugler, F., Lee, S. K., & Papathanassiou, K. P. (2009). Tropical-forest-parameter estimation by means of Pol-InSAR: The INDREX-II campaign. *IEEE Transactions on Geoscience and Remote Sensing*, *47*, 481–493.
Hamilton, S. D., Brodie, G., & O'Dwyer, C. (2005). Allometric relationships for estimating biomass in grey box (*Eucalyptus microcarpa*). *Australian Forestry*, *68*, 267–273.
Harrell, P. A., Bourgeau-Chavez, L. L., Kasischke, E. S., French, N. H. F., & Christensen, N. L. (1995). Sensitivity of ERS-1 and JERS-1 radar data to biomass and stand structure in Alaskan boreal forest. *Remote Sensing of Environment*, *54*, 247–260.
Harrell, P. A., Kasischke, E. S., Bourgeau-Chavez, L. L., Haney, E. M., & Christensen, N. L. (1997). Evaluation of approaches aboveground biomass in using SIR-C data to estimating southern pine forests. *Remote Sensing of Environment*, *59*, 223–233.
Holt, D., Steel, D., Tranmer, M., & Wrigley, N. (1996). Aggregation and ecological effects in geographically based data. *Geographical Analysis*, *28*, 244–261.
Hug, C., Ullrich, A., & Grimm, A. (2004). Litemapper-5600 — A waveform digitising lidar terrain and vegetation mapping system. *International Archives of Photogrammetry, Remote Sensing and Spatial Information Science*, *36*, 24–29.
Imhoff, M. L. (1995). Radar backscatter and biomass saturation: Ramifications for global biomass inventory. *IEEE Transactions on Geoscience and Remote Sensing*, *33*, 511–518.
Kasischke, E. S., Christensen, N. L., & Bourgeau-Chavez, L. L. (1995). Correlating radar backscatter with components of biomass in loblolly pine forests. *IEEE Transactions on Geoscience and Remote Sensing*, *33*, 643–659.
Le Toan, T., Beaudoin, A., & Guyon, D. (1992). Relating forest biomass to SAR data. *IEEE Transactions on Geoscience and Remote Sensing*, *30*, 403–411.
Lee, J. S., Grunes, M. R., Schuler, D. L., Pottier, E., & Ferro-Famil, L. (2006). Scattering-model-based speckle filtering of polarimetric SAR data. *IEEE Transactions on Geoscience and Remote Sensing*, *44*, 176–187.
Lefsky, M.A., Harding, D. J., Keller, M., Cohen, W. B., Carabajal, C. C., Espirito-Santo, F. D. B., et al. (2005). Estimates of forest canopy height and aboveground biomass using ICESat. *Geophysical Research Letters*, *32*, 1–4.
Lu, D. (2006). The potential and challenge of remote sensing-based biomass estimation. *International Journal of Remote Sensing*, *27*, 1297–1328.
Lucas, R., Armston, J., Fairfax, R., Fensham, R., Accad, A., Carreiras, J., et al. (2010). An evaluation of the ALOS PALSAR L-band backscatter — Above ground biomass relationship Queensland, Australia: Impacts of surface moisture condition and vegetation structure. *IEEE Journal of Selected Topics in Applied Earth Observation and Remote Sensing*, *3*, 576–593.
Lucas, R., Milne, A. K., Cronin, N., Witte, C., & Denham, R. (2000). The potential od synthetic aperture radar (SAR) for quantifying the biomass of Australia's woodlands. *The Rangeland Journal*, *22*, 124–140.
Lucas, R., Moghaddam, M., & Cronin, N. (2004). Microwave scattering from mixed-species forests, Queensland, Australia. *IEEE Transactions on Geoscience and Remote Sensing*, *42*, 2142–2159.
MacLean, G. A., & Krabill, W. B. (1986). Gross merchantable timber volume estimation using an airborne LiDAR system. *Canadian Journal of Remote Sensing*, *12*, 7–18.
Maghsoudi, Y., Collins, M., & Leckie, D.G. (2012). Polarimetric classification of Boreal forest using nonparametric feature selection and multiple classifiers. *International Journal of Applied Earth Observation and Geoinformation*, *19*, 139–150.
Mascaro, J., Detto, M., Asner, G. P., & Muller-Landau, H. C. (2011). Evaluating uncertainty in mapping forest carbon with airborne LiDAR. *Remote Sensing of Environment*, *115*, 3770–3774.
Mitchard, E. T. A., Saatchi, S. S., Woodhouse, I. H., Nangendo, G., Ribeiro, N. S., Williams, M., et al. (2009). Using satellite radar backscatter to predict above-ground woody biomass: A consistent relationship across four different African landscapes. *Geophysical Research Letters*, *36*, 1–6.
Moreau, S., & Le Toan, T. (2003). Biomass quantification of Andean wetland forages using ERS satellite SAR data for optimizing livestock management. *Remote Sensing of Environment*, *84*, 477–492.
Morel, A.C., Saatchi, S. S., Malhi, Y., Berry, N. J., Banin, L., Burslem, D., et al. (2011). Estimating aboveground biomass in forest and oil palm plantation in Sabah, Malaysian Borneo using ALOS PALSAR data. *Forest Ecology and Management*, *262*, 1786–1798.
Nelson, R., Swift, R., & Krabill, W. (1988). Using airborne lasers to estimate forest canopy and stand characteristics. *Journal of Forestry*, *86*, 31–38.
Neumann, M., Saatchi, S. S., Ulander, L. M. H., & Fransson, J. E. S. (2012). Assessing performance of L- and P-band polarimetric interferometric SAR data in estimating boreal forest above-ground biomass. *IEEE Transactions on Geoscience and Remote Sensing*, *50*, 714–726.
Nonaka, T., Ishizuka, Y., Yamane, N., Shibayama, T., Takagishi, S., & Sasagawa, T. (2008). Evaluation of the geometric accuracy of TerraSAR-X. *Remote sensing and spatial information sciences*. Beijing: The International Archives of the Photogrammetry.
Openshaw, S. (1984). The modifiable areal unit problem. *Concepts and Techniques in Modern Geography*, *38*, 41.
Panciera, R., Walker, J. P., Jackson, T. J., Ryu, D., Gray, D., Monerris, A., et al. (2013). The Soil Moisture Active Passive Experiments (SMAPEx): Towards soil moisture retrieval from the SMAP mission. *IEEE Transactions on Geoscience and Remote Sensing*, *51*.
Pulliainen, J. T., Kurvonen, L., & Hallikainen, M. T. (1999). Multitemporal behavior of L- and C-band SAR observations of boreal forests. *IEEE Transactions on Geoscience and Remote Sensing*, *37*, 927–937.
Pulliainen, J. T., Mikkela, P. J., Hallikainen, M. T., & Ikonen, J. P. (1996). Seasonal dynamics of C-band backscatter of boreal forests with applications to biomass and soil moisture estimation. *IEEE Transactions on Geoscience and Remote Sensing*, *34*, 758–770.
Ranson, K. J., Saatchi, S. S., & Sun, G. (1995). Boreal forest ecosystem characterization with SIR-C/XSAR. *IEEE Transactions on Geoscience and Remote Sensing*, *33*, 867–876.
Rignot, E. J., Way, J., Williams, C., & Viereck, L. (1994). Radar estimates of aboveground biomass in boreal forests of interior Alaska. *IEEE Transactions on Geoscience and Remote Sensing*, *32*, 1117–1124.
Rignot, E. J., Zimmermann, R., & van Zyl, J. J. (1995). Spaceborne applications of P band imaging radars for measuring forest biomass. *IEEE Transactions on Geoscience and Remote Sensing*, *33*, 1162–1169.
Robinson, C., Saatchi, S. S., Neumann, M., & Gillespie, T. (2013). Impacts of spatial variability on aboveground biomass estimation from L-band radar in a temperate forest. *Remote Sensing*, *5*, 1001–1023.
Saatchi, S. S., Halligan, K., Despain, D.G., & Crabtree, R. L. (2007). Estimation of forest fuel load from radar remote sensing. *IEEE Transactions on Geoscience and Remote Sensing*, *45*, 1726–1739.
Saatchi, S. S., Houghton, R. A., Dos Santos, A., Soares, J. V., & Yu, Y. (2007). Distribution of aboveground live biomass in the Amazon basin. *Global Change Biology*, *13*, 816–837.
Saatchi, S. S., Marlier, M., Chazdon, R. L., Clark, D. B., & Russell, A. E. (2011). Impact of spatial variability of tropical forest structure on radar estimation of aboveground biomass. *Remote Sensing of Environment*, *115*, 2836–2849.
Sandberg, G., Ulander, L. M. H., Fransson, J. E. S., Holmgren, J., & Le Toan, T. (2011). L- and P-band backscatter intensity for biomass retrieval in hemiboreal forest. *Remote Sensing of Environment*, *115*, 2874–2886.
Santoro, M., Beer, C., Cartus, O., Schmullius, C., Shvidenko, A., McCallum, I., et al. (2011). Retrieval of growing stock volume in boreal forest using hyper-temporal series of Envisat ASAR ScanSAR backscatter measurements. *Remote Sensing of Environment*, *115*, 490–507.

Santoro, M., Eriksson, L., Askne, J., & Schmullius, C. (2006). Assessment of stand-wise stem volume retrieval in boreal forest from JERS-1 L-band SAR backscatter. *International Journal of Remote Sensing*, *27*, 3425–3454.

Santoro, M., Fransson, J. E. S., Eriksson, L. E. B., Magnusson, M., Ulander, L. M. H., & Olsson, H. (2009). Signatures of ALOS PALSAR L-band backscatter in Swedish forest. *IEEE Transactions on Geoscience and Remote Sensing*, *47*, 4001–4019.

Tanase, M.A., de la Riva, J., Santoro, M., Le Toan, T., & Perez-Cabello, F. (2010). Sensitivity of X-, C- and L-band SAR backscatter to fire severity in Mediterranean pine forests. *IEEE Transactions on Geoscience and Remote Sensing*, *48*, 3663–3675.

Tanase, M.A., Le Toan, T., de la Riva, J., & Santoro, M. (2009). *An estimation of change in forest area in central Siberia using multi temporal SAR data.* ALOS PI 2008 Symposium. Rhodes, Greece: European Space Agency.

Tanase, M.A., Panciera, R., Lowell, K., Aponte, C., Hacker, J. M., & Walker, J. P. (2014). Forest biomass estimation at high spatial resolution: Radar vs lidar sensors. *IEEE Transactions on Geoscience and Remote Sensing Letters*, *11*, 711–715.

Tanase, M.A., Panciera, R., Lowell, K., Tian, S., Garcia-Martin, A., & Walker, J. P. (2014). Sensitivity of L-band radar backscatter to forest biomass in semi-arid environments: A comparative analysis of parametric and non-parametric models. *IEEE Transactions on Geoscience and Remote Sensing*, *99*, 1–15 (in press).

Tanase, M.A., Santoro, M., Wegmüller, U., de la Riva, J., & Perez-Cabello, F. (2010). Properties of X-, C- and L-band repeat-pass interferometric SAR coherence in Mediterranean pine forests affected by fires. *Remote Sensing of Environment*, *114*, 2182–2194.

Tebaldini, S., & Rocca, F. (2012). Multibaseline polarimetric SAR tomography of a boreal forest at P- and L-bands. *IEEE Transactions on Geoscience and Remote Sensing*, *50*, 232–246.

Trisasongko, B. H. (2010). The use of polarimetric SAR data for forest disturbance monitoring. *Sensing and Imaging*, *11*, 1–13.

Unwin, D. J. (1996). GIS, spatial analysis and spatial statistics. *Progress in Human Geography*, *20*.

van Zyl, J. J., Arii, M., & Kim, Y. (2011). Model-based decomposition of polarimetric SAR covariance matrices constrained for nonnegative eigenvalues. *IEEE Transactions on Geoscience and Remote Sensing*, *49*, 3452–3459.

Wegmüller, U., Werner, C., Strozzi, T., & Wiesmann, A. (2002). Automated and precise image registration procedures. In L. Bruzzone y, & P. Smits (Eds.), *Analysis of multi-temporal remote sensing images* (pp. 37–49). Singapore: World Scientific.

Yague-Martinez, N., Eineder, M., Xiao Ying, C., & Minet, C. (2012). Ground displacement measurement by TerraSAR-X image correlation: The 2011 Tohoku-Oki earthquake. *Geoscience and Remote Sensing Letters, IEEE*, *9*, 539–543.

Yamaguchi, Y., Moriyama, T., Hiroyoshi, M. I., & Shinji, Y. (2005). Four-component scattering model for polarimetric SAR image decomposition. *IEEE Transactions on Geoscience and Remote Sensing*, *43*, 1699–1706.

Zolkos, S. G., Goetz, S. J., & Dubayah, R. (2013). A meta-analysis of terrestrial aboveground biomass estimation using lidar remote sensing. *Remote Sensing of Environment*, *128*, 289–298.